A 2.13 Å Structure of *E. coli* Dihydrofolate Reductase Bound to a Novel Competitive Inhibitor Reveals a New Binding Surface Involving the M20 Loop Region

Rachael L. Summerfield,[†] Denis M. Daigle,[‡] Stanislas Mayer,[§] Debasis Mallik,[§] Donald W. Hughes,[||] Sean G. Jackson,[⊥] Margaret Sulek,[⊥] Michael G. Organ,[§] Eric D. Brown,[⊥] and Murray S. Junop*[,⊥]

Atlantic Veterinary College, University of Prince Edward Island, 550 University Avenue, Charlottetown, Prince Edward Island C1A 4P3, Canada, Novartis Institutes for Biomedical Research, 100 Technology Square, Cambridge, Massachusetts 02139, Department of Chemistry, York University, 4700 Keele Street, Toronto, Ontario M3J 1P3, Canada, Department of Chemistry, McMaster University, 1200 Main Street West, Hamilton, Ontario L8S 4M1, Canada, and Department of Biochemistry and Biomedical Sciences, McMaster University, 1200 Main Street West, Hamilton, Ontario L8N 3Z5, Canada

Received May 12, 2006

Dihydrofolate reductase (DHFR) is a vital metabolic enzyme and thus a clinically prominent target in the design of antimetabolites. In this work, we identify 1,4-bis-{[*N*-(1-imino-1-guanidino-methyl)]sulfanylmethyl}-3,6-dimethyl-benzene (compound **1**) as the correct structure of the previously reported DHFR inhibitor 1,4-bis-{(iminothioureidomethyl)aminomethyl}-3,6-dimethyl-benzene (compound **2**). The fact that compound **1** has an uncharacteristic structure for DHFR inhibitors, and an affinity (K_I of 11.5 nM) comparable to potent inhibitors such as methotrexate and trimethoprim, made this inhibitor of interest for further analysis. We have conducted a characterization of the primary interactions of compound **1** and DHFR using a combination of X-ray structure and SAR analysis. The crystal structure of *E. coli* DHFR in complex with compound **1** and NADPH reveals that one portion of this inhibitor exploits a unique binding surface, the M20 loop. The importance of this interface was further confirmed by SAR analysis and additional structural characterization.

Introduction

Dihydrofolate reductase (DHFR;[a] EC 1.5.1.3) catalyzes the NADPH-dependent reduction of dihydrofolate to tetrahydrofolate.[1] Tetrahydrofolate, and other reduced folates, are critical cofactors for a number of one-carbon transfer reactions including those important in the biosynthesis of purines, thymidylate, panthothenate, and some amino acids (reviewed in refs 2 and 3). DHFR is therefore a popular target for small molecule therapeutics aimed at a variety of diseases including cancer, malaria, and bacterial infection. Because of the importance of DHFR as a therapeutic target, the structure, mechanism, and inhibition of the *E. coli* enzyme have been the subject of intensive study. There have been comprehensive investigations of inhibition of DHFR by methotrexate[4] and by diaminobenzylpyrimidines such as trimethoprim.[5] A complete kinetic and thermodynamic description of the reaction pathway has been presented,[6] in addition to an analysis of key loop and subdomain movements along the reaction pathway depicted by six isomorphous crystallographic structures.[7]

Recently, we reported on a high-throughput screen of 50 000 structurally diverse small molecules against *E. coli* dihydrofolate reductase to detect new inhibitors.[8] This screen revealed nine molecules that were competitive with dihydrofolate and had not been characterized previously as inhibitors of DHFR. Most of these inhibitors were 2,4-diaminoquinazolines and 2,4-diaminopyrimidines, structural classifications commonly associated with activity against DHFR (reviewed in ref 9). One molecule (compound **2**), however, was relatively potent (26 nM) and structurally unusual as an inhibitor of DHFR in its lack of a diaminoheterocycle. In the work reported here, we determined that a structural isomer of compound **2**, compound **1** (Chart 1), was in fact the identity of the active molecule and not the previously reported structure of compound **2**. Compound **1** is likewise a novel and unusual inhibitor of DHFR. The molecule has a paradimethylbenzene core symmetrically substituted with two identical isothiourea groups. We therefore sought to understand the inhibition of DHFR by compound **1** through studying structure/activity relationships (SAR) of a series of structural analogues. In addition, high-resolution X-ray co-structures of DHFR with compound **1** and a monosubstituted analogue have revealed a mode of interaction of the inhibitor with DHFR not previously observed. While compound **1** benefits from some interactions analogous to those of other well-characterized DHFR inhibitors, it makes substantial contacts with and derives significant binding energy from interactions with the M20 loop region of DHFR, a heretofore unexploited binding surface for the inhibition of this enzyme.

Results and Discussion

Structural Identification of Compound 1. During initial stages of structure refinement of the ternary complex of DHFR−NADPH−compound **2**, it became apparent that the structure of compound **2** as originally reported[8] could not be readily modeled into the available electron density. Because the X-ray diffraction data used during this stage of refinement were collected to 1.89 Å resolution, it was possible to use anomalous signal from sulfur atoms to help position the inhibitor within electron density maps. Analysis of the anomalous signal strongly suggested that the annotated structure for compound **2** had assigned both sulfur atoms within the inhibitor incorrectly (compare compounds **2** and **1** in Chart 1). To further confirm

* To whom correspondence should be addressed. Tel.: 905 525-9140 x 22912. Fax: 905 522-9130. E-mail: junopm@mcmaster.ca.
[†] Atlantic Veterinary College, University of Prince Edward Island.
[‡] Novartis Institutes of Biomedical Research.
[§] Department of Chemistry, York University.
[||] Department of Chemistry, McMaster University.
[⊥] Department of Biochemsitry and Biomedical Sciences, McMaster University.

[a] Abbreviations: DHFR, dihydrofolate reductase; SAR, structure activity relationship; NADPH, nicotinamide adenine dinucleotide phosphate; THF, tetrahydrofolate; rms, route mean square; PEG, polyethylene glycol; FID, flame ionization detector; HSQC, heteronuclear single quantum correlation; HMBC, heteronuclear multiple bond correlation.

10.1021/jm060570v CCC: $33.50
Published on Web 11/04/2006

Chart 1

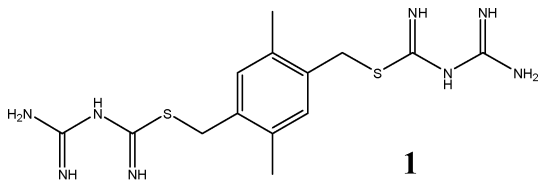

1

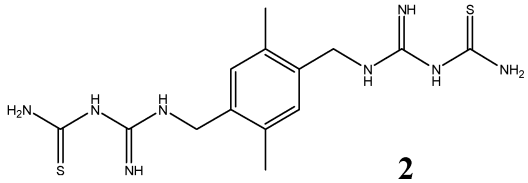

2

Table 1. Comparison of Predicted and Measured ^{13}C Chemical Shifts for the C-7 Methylene Group of Compounds **1** and **2**

compound	atom bonded to C-7 methylene	predicted ^{13}C chemical shift (ppm)	obtained ^{13}C chemical shift (ppm)
1	S	29.47	32.81
2	N	45.91	

our X-ray data, we analyzed the structure of compound **2** by NMR. Carbon chemical shifts were assigned from the correlations detected in the HSQC and HMBC spectra (see Supporting Information). Quaternary carbons on the aromatic ring could not be definitely assigned due to their similar chemical shifts and identical HMBC correlations with both neighboring aromatic and aliphatic protons.

The carbon chemical shift of the C-7 methylene group at 32.81 ppm was more consistent with a structure where the sulfur atom was bonded to the methylene carbon based on calculations using ACD Labs ^{13}C chemical shift prediction software (ver. 5.09) (Table 1). The methylene carbon chemical shift was predicted to be 29.47 ppm in the CH_2-S case versus 45.91 ppm in the CH_2-N form of the compound (Table 1). If a nitrogen atom were attached to the C-7 methylene group, a higher frequency chemical shift would be expected for the methylene carbon because of the inductive effect of the more electronegative nitrogen relative to the sulfur. It was therefore concluded that compound **2** contained in fact a sulfur bonded methylene and that it be designated as compound **1** in future discussions.

SAR data further supported the structure of compound **1**, as none of the 20 second-generation inhibitors synthesized based on the compound **2** structure exhibited any detectable inhibitory activity.[10] However, as outlined below, when inhibitors were synthesized on the basis of the compound **1** structure, significant inhibitory activity was observed.

DHFR−Compound 1 Structure. The crystal structure of DHFR bound to compound **1** was determined to 2.13 Å resolution (see Experimental Section). Conditions used for cocrystallization were similar to those previously reported by Sawaya and Kraut (1997) and resulted in crystals that grew in the same space group ($P2_12_12_1$) with similar unit cell parameters. We chose these conditions because they had been successfully used to grow isomorphous cocrystals of DHFR complexes representing essentially every kinetic intermediate in the DHFR reaction coordinate. By obtaining the structure of DHFR bound to compound **1** under similar conditions, we anticipated being able to make comparisons with these structures while avoiding uncertainties associated with comparing structures determined in different space groups.

The overall ternary structure of DHFR in complex with NAPDH and compound **1** is similar to previously determined structures of DHFR, and therefore only a stereoview of the substrate binding pocket region is presented in Figure 1. Main chain (I5, A7, S49, I94) and side chain atoms (M20, D27, F31, I50, Y100, T113) directly contributing to substrate binding are shown in Figure 1. In addition to these binding contacts, several water molecules (W603, W716, W770, W876, W925) implicated in substrate interactions are also indicated. The final model was refined to R and R_{free} values of 23.3 and 25.6, respectively. A complete list of data collection and model refinement statistics is presented in Table 2.

As shown in Figure 1, electron density covering compound **1** was clearly observed within the folate binding cleft formed between helices B and C of DHFR. The inhibitor makes significant interactions with DHFR, burying 760.4 Å^2 of surface area. A considerable portion of this interaction results from binding to the same surface of DHFR that accommodates the pteridine ring system of dihydrofolate. However, greater than one-third of the total surface area buried by compound **1** results from interactions not previously observed in either substrate or inhibitor binding. Because the structure of compound **1** is symmetrical, we have designated the regions that interact with the pteridine ring binding pocket and M20 loop as the proximal and distal isothiourea groups, respectively. The proximal region of compound **1** makes direct interactions with residues I5, A7, M20, D27, F31, I94, Y100, and T113, while the distal portion of compound **1** makes specific interactions with residues S49 and I50 as well as van der Waals contacts with A19, M20, L28, S49, I50, and NADPH.

Although surface area calculations indicate that significant interactions are made between DHFR and inhibitor through the distal portion of compound **1**, our data more accurately suggest that the majority of binding energy occurs as a result of contacts made with the proximal region. When electron density maps are contoured at high σ values ($>3\sigma$), electron density is primarily limited to the proximal portion of the inhibitor reflecting stronger, more stable interactions. In addition, average *B*-factors of side chain atoms making direct contacts with the proximal region of compound **1** are 2.23-fold lower than those interacting with the distal region, indicating tighter binding between DHFR and the proximal portion of the inhibitor.

Structural comparison of the ternary DHFR−NADPH−inhibitor complex with six isomorphous structures[7] was carried out to further characterize interactions of DHFR and compound **1**. Five structures representing different kinetic intermediates (NADPH, PDB 1rx1; NADPH/DHF, PDB 1rx2; NADP+/THF, PDB 1rx4; THF, PDB 1rx5; and NADPH/THF, PDB 1rx6) as well as a single structure representative of the transition state (NADPH/DHF, PDB 1rx3) were previously reported by Sawaya and Kraut (1997). Each structure was determined under the same crystallization conditions, resulting in crystal packing that permits subdomain rotation and M20 loop movement necessary for substrate binding and catalysis. The M20 loop (residues 10−24) is observed crystallographically in open, closed, or occluded conformations depending on whether the active site is itself open, closed, or occluded by the M20 loop. In structures representative of the holoenzyme, Michaelis complex, and transition state, the M20 loop adopts a closed conformation. Structures representative of NADP+/THF, THF, and NADPH/THF enzyme-bound complexes suggest that the occluded state is favored during later stages of the reaction cycle. The open conformation is believed to represent a more transient structural

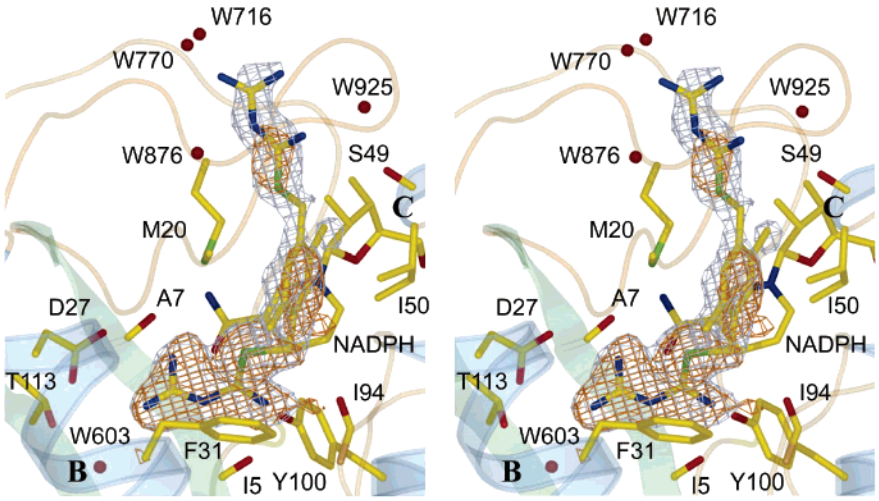

Figure 1. Structural model of compound **1** bound in the active site of DHFR. Helices and strands are labeled in bold according to the nomenclature of Sawaya and Kraut (1997). Secondary structure elements are colored as follows: helices, blue; strands, green; and loops, beige. Atom colors: C, yellow; N, blue; O, red; S, green. An $F_o - F_c$ omit map contoured at 2.5σ and refined $2F_o - F_c$ electron density map contoured at 1σ are shown in orange and blue mesh, respectively. Only residues and water molecules within 3.5 Å of compound **1** are shown and labeled, in addition to NADPH.

Table 2. Data Collection and Model Refinement Statistics for *E. coli* DHFR in Complex with NADPH and Compound **1** or **7**

	compound **1**	compound **7**
data collection		
space group	$P2_12_12_1$	$P2_12_12_1$
unit cell parameters (Å)	$a = 34.0$, $b = 44.7$, $c = 98.1$ $\alpha = \beta = \gamma = 90°$	$a = 34.1$, $b = 44.1$, $c = 97.8$ $\alpha = \beta = \gamma = 90°$
no. of molecules in asymmetric unit	1	1
resolution range (Å)[a]	40.7−1.89 (1.96−1.89)	40.2−2.68 (2.78−2.68)
unique reflections	12 541	4392
data redundancy	2.66	2.66
completeness (%)[a]	98.1 (98.9)	97.8 (100)
$I/\sigma(I)$[a]	8.8 (2.4)	13.1 (4.0)
R_{merge} (%)[a]	7.1 (34.3)	6.2 (20.4)
model and refinement		
resolution range (Å)[a]	25−2.13	40.2−2.68
R_{work} (%)[a]	23.3	23.7
R_{free} (%)[a]	25.6	25.0
no. of reflections	7747 working set 770 test set	3820 working set 448 test set
cutoff criterion	$\|F\|/\sigma F > 2.0$	$\|F\|/\sigma F > 2.0$
no. of amino acid residues/ atoms	159/1268	159/1268
no. of waters	411	118
rmsd bond lengths (Å)[a]	0.021	0.011
rmsd bond angles (deg)[a]	1.9	1.7
average *B*-factor (Å^2)[a]	26.6	38.4
Protein Data Bank ID	2ANQ	2ANO

[a] Values in parentheses are for the highest resolution shell.

transition between closed and occluded conformations. Comparison of the compound **1** ternary structure with the structures determined by Sawaya and Kraut (1997) indicated that the lowest rms deviation (0.80 Å) was achieved by superimposition with the structure representative of the transition state (NADPH/methotrexate, PDB 1rx3). As shown in Figure 2A, no significant differences were observed in conformations of either the main chain or the side chains involved in substrate/inhibitor binding (Figure 2A). In addition, the relative position of NADPH remained unaltered. Thus, structural analysis suggests that, similar to methotrexate (PDB 1rx3), the binding of compound **1** to DHFR−NADPH results in an active site conformation that is representative of the transition state.

The structure of methotrexate closely resembles that of dihydrofolate, and therefore it is not surprising that both occupy essentially identical binding pockets within DHFR (Figure 2B). In contrast, methotrexate and compound **1**, which share only two-thirds of the same binding surface, induce identical conformational changes within DHFR. The proximal region of compound **1** superimposes almost perfectly with the pteridine ring system of methotrexate (Figure 2A). However, unlike the rigid 2,4-diaminopyrimidine ring present in methotrexate, the proximal isothiourea moiety of compound **1** is not constrained by a closed ring system, making this region of the inhibitor conformationally flexible and perhaps better suited for interactions with DHFR. In addition to similarities in the pteridine binding pocket, compound **1** and methotrexate share a central aromatic ring found to be coplanar and present within the hydrophobic cleft formed between residues M20, I50, and F31. In compound **1**, however, the ring is positioned more closely toward the bound NADPH molecule because of further interactions made through its distal thiourea group.

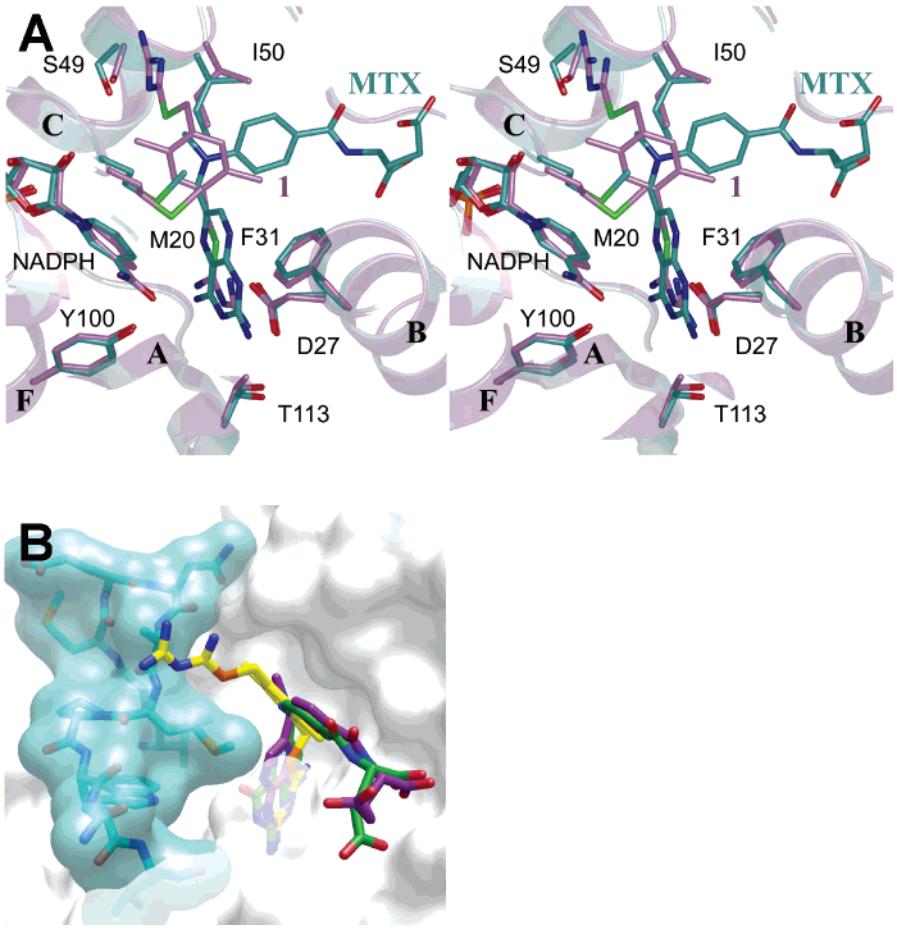

Figure 2. Superimposition of compound **1**, dihydrofolate, and methotrexate in complex with NADPH-bound DHFR. (A) Structural comparison of compound **1** and methotrexate in complex with DHFR. Atoms are colored as in Figure 1, excluding carbon atoms, which are colored magenta for the compound **1** model and cyan for the methotrexate model. NADPH is colored magenta or cyan accordingly. Only residues directly implicated in inhibitor binding are shown and labeled. (B) Surface area representation of DHFR with compound **1**, dihydrofolate, and methotrexate shown in yellow, purple, and green stick, respectively. The M20 loop residues 10−24 and molecular surface are indicated in cyan.

Although at first glance the structure of compound **1** with its central aromatic ring and symmetrically opposed isothiourea moieties does not resemble dihydrofolate or standard inhibitors containing 2,4-diaminopyrimidine rings, closer examination of this compound bound within the active site of DHFR reveals some significant similarities. In particular, all of the nitrogen atoms within the proximal isothiourea group of compound **1** superimpose almost perfectly with those located in the pteridine ring system of methotrexate and dihydrofolate. Therefore, although compound **1** is unique in its lack of a rigid 2,4-diaminopyrimidine ring, one of its two flexible isothiourea groups binds in a manner that mimics this ring system, further highlighting the importance of the hydrogen-bonding interactions of these four nitrogen atoms. The interactions of D27, T113, and I5 with the pteridine ring nitrogen atoms of dihydrofolate have been well characterized and demonstrated to be critical for substrate binding and catalysis.[7,11−13] Thus, it is not surprising that the substitution of a less electronegative sulfur atom for nitrogen, as exhibited in the incorrect structure of compound **2** (Table 2), would have negative consequences for the inhibitor's ability to interact with D27. Cummins and Gready (2001) demonstrated 3−4-fold decreases in catalytic efficiency when Asn or Ser replaced Asp27. Given the modest decreases in activity associated with these amino acid substitutions, one would not have expected such dramatic differences in inhibition by compound **2** versus **1** structure. The differences are too large to simply reflect the disruption of a single hydrogen-bonding interaction to D27. Perhaps the observed transition state conformation induced in DHFR by the binding of compound **1** is the result of binding to a transition state analogue.

During the past decade, there has been a significant increase in the amount of structural information available for DHFR. While the most extensively characterized form is derived from *E. coli*, similar structures are now available for many organisms. Of the more than 100 DHFR structures currently deposited in the protein data bank, greater than 50% were determined as complexes with inhibitors, and a significant number of the remainder were bound to substrate or product analogues. What is particularly significant about the compound **1** structure reported here is that it identifies a novel inhibitor-binding surface within DHFR. The vast majority of DHFR inhibitors described in the literature, including the most clinically useful, contain a modified version of the 2,4-diaminopyrimidine ring of dihydrofolate.[14] In this respect, compound **1** can be considered similar because the proximal isothiourea moiety mimics the same binding observed for diaminopyrimidine-containing inhibitors (Figure 2). After an exhaustive search of all inhibitor-bound DHFR structures in the Protein Data Bank, it is apparent that the distal isothiourea group of compound **1** binds in a pocket that is not exploited by any other reported inhibitor for which structural data are available. The distal region of compound **1** extends toward the flexible M20 loop, making hydrogen bonds with several ordered water molecules as well as residue S49 of helix C and the main chain atoms of residue 20. In addition,

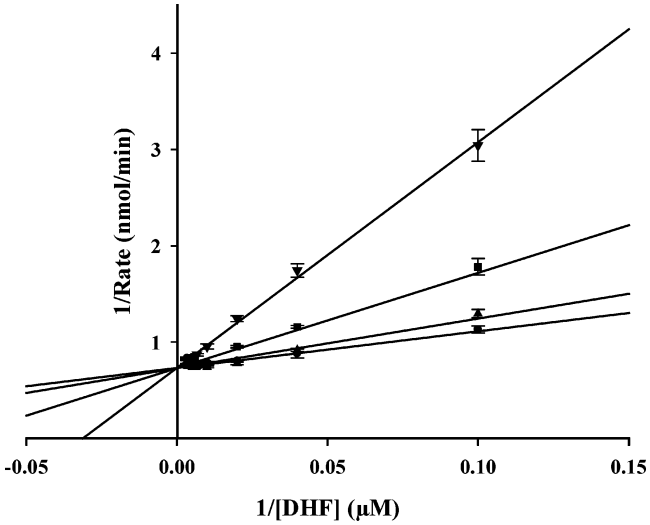

Figure 3. Compound **1** is a competitive inhibitor of *E. coli* DHFR. Lineweaver−Burk plots at four concentrations of compound **1**, 2.5, 7.5, 25, and 75 nM, display competitive inhibition behavior toward dihydrofolate with an inhibition constant (K_I) of 11.5 nM. Plots were generated using Sigmaplot version 8.0 software. Assays (200 μL) were performed at 25 °C in 50 mM Tris-HCl, pH 7.5, containing 0.01% (w/v) Triton X-100, and 10 mM 2-mercaptoethanol as described in the Experimental Section.

there are a number of carbonyl oxygen atoms located along the extended binding cleft that could be exploited. If the distal isothiourea moiety of compound **1** was extended by the addition of even one methylene group following the aromatic ring, the resulting compound could make additional stabilizing hydrogen bonds with DHFR. Although binding of the distal portion of compound **1** is weaker than the proximal portion, the fact that it interacts with a novel binding surface of DHFR suggests the potential for further exploitation in the development of new potent DHFR inhibitors.

Compound 1 Structure−Activity Analysis. In a preliminary mechanistic analysis, compound **1** was judged to be competitive with the substrate dihydrofolate based on IC_{50} determinations at two different substrate concentrations.[8] Figure 3 depicts a thorough steady-state mechanistic analysis of inhibition by compound **1**, confirming the competitive behavior with respect to dihydrofolate that is consistent with the co-structural studies presented here.

To further analyze the overall contribution of the distal isothiourea group of compound **1** toward DHFR binding as well as to explore other potential binding pocket interactions, a set of 17 related compounds were synthesized and tested for their ability to inhibit DHFR activity. These inhibitors were designed to maintain the interaction of the proximal isothiourea group while replacing the distal isothiourea with a variety of functional groups.

The amidinothiouronium collection was prepared by one of four protocols (Scheme 1) that provided the desired compounds in one synthetic operation (see Experimental Section and Supporting Information). A variety of commercially available benzyl chloride reagents were reacted with amidinothiourea to obtain the benzyl isothioamidine library. To prepare these compounds quickly and in high purity, a microwave-mediated process was developed using a Smith Synthesizer. A number of reaction conditions were evaluated using both protic and aprotic polar solvents under a wide range of reaction temperatures (60−150 °C). Although thioalkylations were found to be facile at higher temperatures, degradation of the products to their corresponding thiols was a serious concern. Short-duration

Scheme 1[a]

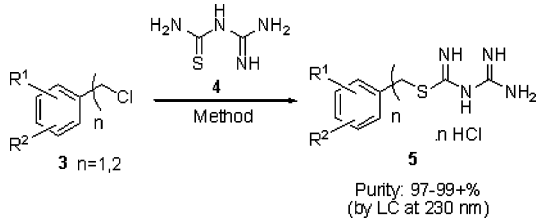

[a] Method A: (a) **3** (1.0 equiv), MeCN, microwave, 85−100 °C, 5 min; (b) filter. Method B: (a) **3** (1.0 equiv), MeOH, microwave, 20 °C, 10 min; (b) filter. Method C: (a) **3** (1.0 equiv), MeOH, microwave, 60 °C, 20 min; (b) 3 N HCl_{aq}; (c) filter. Method D: (a) **3** (2.0 equiv), EtOH, microwave, 90 °C, 5 min; (b) filter.

microwave irradiation methods were found to be effective, and, in many cases, the hydrochloride salts of the desired products precipitated out of solution in high purity. For certain benzyl chlorides, methanol was found to be a better solvent when the microwave irradiation was performed at a moderate temperature (60 °C). In the case of perfluorinated derivatives (i.e., CF_3-containing derivatives), addition of aqueous hydrochloric acid was necessary to initiate the precipitation of the salt. For the preparation of the disubstituted derivatives, ethanol was the most effective solvent. A detailed description of the individual methods along with all LCMS and NMR spectra can be found in the Supporting Information. The choice to use one protocol over another was determined individually on the basis of the solubility of the desired product and the presence of impurities. As outlined in Table 3, yields were moderate to good, and purities were all excellent (>96%). The structures, classification, and IC_{50} values of these inhibitors are presented in Table 3.

Comparison of the IC_{50} values for the 17 amidinothiouronium compounds analyzed revealed several general features about binding interactions of the benzyl group with DHFR. First, the presence of just a benzyl group (compound **9**) resulted in less effective binding as compared to essentially all other types of benzyl substitutions tested. This observation suggests that to maximize interactions with the binding surface cleft (I50, F31, M20, and NADPH) of DHFR, inhibitors must have some benzyl derivatization. The only exception was the addition of a large CF_3 group at the 2-position as observed in compound **18**. In this case, some steric hindrance would be unavoidable without further altering interactions with the proximal isothiourea moiety. This alteration resulted in the poorest binding of all compounds tested, underscoring the detrimental consequences of steric clashes in general. Second, the spacing between proximal isothiourea and benzyl groups is already close to optimal in compound **1**. Increasing this distance by the insertion of two carbon atoms (compound **20**) resulted in decreased inhibition. Although not tested, it would be interesting to determine the effect of inserting a single carbon at this position in the context of an otherwise intact compound **1**. The ternary structure of compound **1** in complex with DHFR and NADPH suggested that the distal isothiourea group could adopt more optimal interactions with several carbonyl groups in the M20 loop if it was on a slightly longer tether from the anchoring proximal isothiourea moiety. Third, the presence of hydrophobic groups at both the 3 and the 4 positions of benzene is preferential for binding. This finding is consistent with the hydrophobic nature of the I50−M20 binding cleft.

Although all second-generation inhibitors displayed IC_{50} levels higher than that of compound **1**, the observed increases in IC_{50} values only spanned a relatively narrow range of ∼50−500-fold, suggesting that the majority of binding interactions

Table 3. Structure−Activity Relationship Analysis of Compound **1**

General structure and class	Compound name	Substitution R1	Substitution R2	Protocol[a] (temp) solvent	Yield (mg)	Purity[b] (%)	IC_{50}[a] (μM)
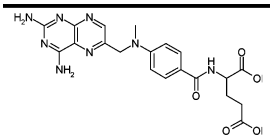	methotrexate	-	-	-	-	-	0.003 ± 0.0001
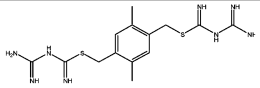	**1**	—	—	[e]D (90 °C) Ethanol	78	98	0.075 ± 0.006
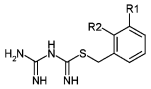	**6**	OCH_3	H	[c]B (60 °C) MeOH	64	99	3.8 ± 0.2
	7	CF_3	H	[c]B (60 °C) MeOH	27	99	4.3 ± 0.4
	8	NO_2	H	[c]B (60 °C) MeOH	49	99	18.9 ± 3.2
	9	H	H	[c]B (60 °C) MeOH	61	99	34.6 ± 6.2
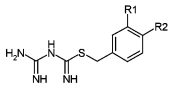	**10**	H	OCH_3	A (90°C) CH_3CN	74	99	3.3 ± 0.3
	11	Cl	Cl	[c]B (60 °C) MeOH	49	99	3.7 ± 0.4
	12	H	CH_3	A (95°C) CH_3CN	52	99	12.6 ± 1.1
	13	H	CF_3	[d]C (60 °C) MeOH	25	99	13.0 ± 1.3
	14	H	Cl	A (100°C) CH_3CN	37	99	14.2 ± 1.8
	15	H	F	[c]B (60 °C) MeOH	47	99	24.9 ± 3.7
	16	H	NO_2	[c]B (60 °C) MeOH	49	99	35.1 ± 6.5
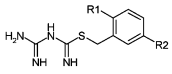	**17**	OH	NO_2	A (90°C) CH_3CN	86	99	15.1 ± 2.0
	18	CF_3	H	[d]C (60 °C) MeOH	17	99	40.6 ± 9.1
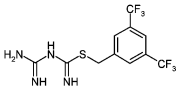	**19**	—	—	[d]C (60 °C) MeOH	7	99	5.6 ± 0.5
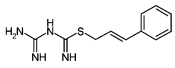	**20**	—	—	A (85°C) CH_3CN	57	99	19.8 ± 2.9
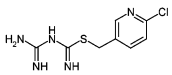	**21**	—	—	[c]B (60 °C) MeOH	63	96	34.7 ± 8.3
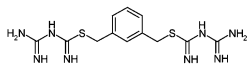	**22**	—	—	[e]D (90 °C) Ethanol	72	97	0.075 ± 0.006

[a] For all reactions, the benzyl chloride and amidinothiourea were mixed together (1:1) in solvent and irradiated at various temperatures for 5 min in a Smith Synthesizer microwave. The products were then collected by recrystallization. [b] Purity was determined by LCMS (λ = 230 nm). [c] Methanol was removed after irradiation and the residue reconstituted in CH_3CN where the product slowly recrystallized. [d] Methanol was removed after irradiation and the residue reconstituted in ether where the product slowly recrystallized. [e] Ethanol was used as the solvent, and the product was collected by simple filtration of crystallized material from the reaction medium.

utilized by these inhibitors was still largely dependent on their common isothiourea moiety. The X-ray structure of a single representative inhibitor, **7**, was subsequently determined to further test the hypothesis that the general reduction in binding observed for all second-generation inhibitors was the result of the loss of the distal isothiourea group and not simply altered

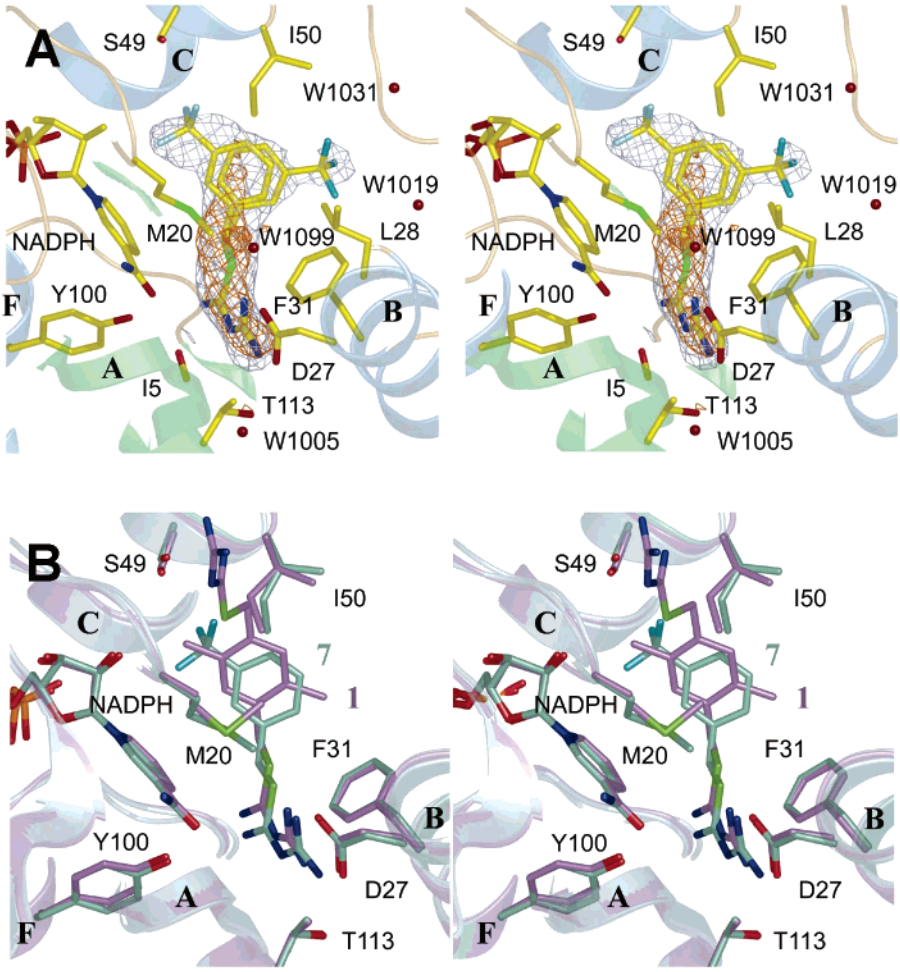

Figure 4. Structural model of DHFR in complex with inhibitor **7**. Atoms and secondary structure elements are colored as in Figure 1, in addition to fluorine atoms, which are shown in turquoise. An $F_o - F_c$ omit map contoured at 2.5σ and refined $2F_o - F_c$ electron density map contoured at 1σ are shown in orange and blue mesh, respectively. Only residues and water molecules within 3.5 Å of **7** are shown and labeled, in addition to NADPH. (A) Electron density maps of **7** bound in the active site of DHFR. (B) Superimposition of **1** and **7** in complex with NADPH-bound DHFR. **7** is shown in cyan and **1** in magenta.

binding of the proximal isothiourea moiety common to all inhibitors tested.

Crystals were generated for the DHFR−NADPH−**7** complex using the same conditions used for the compound **1** complex. The final model was refined to a resolution of 2.68 Å. General data collection and model refinement statistics are presented in Table 2. Well-defined electron density was evident for molecule **7** bound in the active site of DHFR (Figure 4A). As suggested by the SAR binding data, the isothiourea group of this inhibitor was bound at the same place within the active site occupied by the proximal region of compound **1** (Figure 4B). As shown in the final refined electron density map, there was clear evidence for an alternate conformation for the central aromatic ring of **7** involving a 180° rotation (Figure 4A). The most favored conformation, displaying the greatest proportion of electron density in Figure 4A, is positioned in the same overall direction adopted by compound **1** (Figure 4B). That this alternate conformation was observed is consistent with the observation that compound **19** exhibited the same degree of inhibition as compound **7**. In addition, the aromatic ring structure of **7** is tilted outward by 30° relative to the aromatic ring of compound **1**. This permits the fluorine atoms to be positioned in the same location as is occupied by several atoms of the central aromatic ring of compound **1**. Comparison of the ternary structures determined with either compound **1** or **7** reveals very little difference in the overall mode of inhibitor binding. This further supports the idea that the general increase in IC_{50} levels observed for second-generation inhibitors can be attributed largely to the loss of binding interactions with the distal isothiourea group of compound **1**. The average main-chain *B*-factor for the DHFR−NADPH−**7** complex is 33.7 Å,^{2} as compared to 20.2 and 16.4 Å^2 for the same structures determined in the presence of compound **1** and methotrexate, respectively. The higher overall *B*-factor may relate in part to the lower resolution of the data and increased disorder within this crystal; however, a closer examination of individual *B*-factors reveals that there are several areas in the model where the *B*-factors are significantly higher for the compound **7** structure as compared to that of the compound **1** structure. In particular, residues in the M20 loop (amino acids 10−24) and an adenosine-binding loop (residues 63−66) showed increases in average *B*-factors of ∼50%. These changes in *B*-factors can be directly attributed to the decreased number of interactions made between the M20 loop of DHFR and **7** as compared to compound **1**. Taken together, these observations suggest that the decreased potency of **7** can be ascribed largely to the lack of a second isothiourea group.

Conclusion

Although DHFR has been successfully targeted in the fight against both bacterial infections and cancer, there still exists great potential for the development of new inhibitors directed toward this enzyme. The discovery of new lead inhibitors

sufficiently unrelated to those currently available is paramount in achieving this objective. When compound **1** was initially identified as a potent inhibitor of DHFR,[8] it was already apparent from its uncharacteristic structure that it might interact with DHFR in a unique manner and potentially serve as a novel molecular scaffold upon which more specific inhibitors could be designed. In this work, we have conducted a preliminary characterization of the primary interactions of compound **1** and DHFR using a combination of X-ray structure and SAR analysis. Crystal structure determination of the DHFR−NADPH−compound **1** ternary structure revealed not only the primary interactions of molecules within this complex, but, more importantly, led to the identification of the correct and active structure of compound **1**. The critical nature of this discovery is highlighted by the absolute lack of inhibitory activity observed when second-generation inhibitors were synthesized on the basis of the incorrect structure.

SAR analysis of compound **1** further supports the importance of the novel-binding surface observed in the compound **1** ternary complex structure. In addition, the cocrystal structure for one of the single isothiourea-containing compounds (inhibitor **7**) provided evidence to support the idea that the primary mode of binding exhibited by second-generation inhibitors is through interactions within the pteridine ring binding pocket of DHFR. Conserved DHFR binding interactions with the proximal isothiourea groups of both compounds **1** and **7** suggest that the decreased potency of **7** can be directly attributed to the lack of a second isothiourea group. This is supported by the observations that all second-generation inhibitors tested, which lacked one of the two isothiourea groups of compound **1**, had significantly higher IC_{50} values (50−500 fold), with a narrow range of distribution for this increase of only 10-fold. Thus, it appears that while a single isothiourea group is sufficient to orient compound **1** into the substrate-binding pocket of DHFR, significant binding energy is made available through interactions of the second isothiourea group with the M20 binding pocket.

The inhibitory activity of compound **1** is comparable to that of the most effective drugs targeting DHFR, methotrexate, and trimethoprim. The crystal structure of *E. coli* DHFR in complex with compound **1** and NADPH reported here clearly reveals that one portion of this inhibitor exploits a unique binding surface, the M20 loop binding pocket. Together the high potency, novel structure, and unique mode of binding make compound **1** a promising new inhibitor of DHFR. On the basis of the structures and SAR analysis presented in this work, a defined region of compound **1** can now be targeted for more focused chemical modification to improve its activity.

Experimental Section

Expression and Purification of *E. coli* DHFR. *E. coli* DHFR was expressed in BL21(DE3), using the pFW117.1 vector, and purified using a modified version of a previously described protocol.[1] Briefly, a 2 L cell culture was grown at 37 °C until the OD_{600} was 0.8−1.0, and then induced for 3.5 h at 37 °C by addition of 1 mM IPTG. Harvested cells were resuspended in 500 mM imidazole pH 6.6, 5 mM EDTA, and 10 mM 2-mercaptoethanol with the addition of 1 mM benzamidine, 0.1 μM leupeptin, 1 μM pepstatin, and 1 mM phenylmethyl sulfonyl fluoride. Following lysis by two sequential passages through a French Press at 20 000 psi, the cell lysate was clarified by centrifugation at 40 000*g* for 20 min.

DHFR was precipitated from clarified lysate by addition of ammonium sulfate to a final concentration of 3 M. The precipitate was redissolved and purified on a methotrexate affinity column (Sigma-Aldrich Co.) as previously described.[15] Following SDS-PAGE analysis, fractions containing DHFR were pooled and dialyzed against 2 L of 20 mM imidazole pH 7.6 and 100 mM KCl, exchanged six times during dialysis. Dialyzed protein was loaded onto a Q-Sepharose column (Amersham Biosciences) equilibrated with 20 mM imidazole pH 7.6 and 100 mM KCl. DHFR was eluted in a KCl gradient at approximately 300 mM salt. Buffer was exchanged by ultrafiltration (10K MWCO Macrosep Centrifugal Device, Pall Gelman). Protein concentration was determined using the Bradford reagent (BioRad). Because of its relative insolubility, compound **1** was added at a final concentration of 0.154 mM to 1 mg/mL (0.0514 mM) DHFR. Following the addition of NADPH at 1 mM, the solution was allowed to incubate at 4 °C overnight. The protein-inhibitor solution was concentrated to 10 mg/mL.

Crystallization and Structure Determination. All crystals of DHFR in complex with compound **10a** and NADPH were grown using the hanging drop/vapor diffusion method at 20 °C, a reservoir volume of 500 μL, and a drop containing 1 μL of complex and 1 μL of mother liquor. The reservoir solution consisted of 20 mM imidazole pH 8.0, 300 mM $CaCl_2$, and 25% PEG 6000. Crystals grew to a final size of 700 × 100 × 50 μm^3 within 3−4 days. Prior to data collection, crystals were soaked for approximately 30 s in cryo-protecting solution (20 mM imidazole pH 8.0, 300 mM $CaCl_2$, 25% PEG 6000, 30% glycerol) and then flash frozen in liquid nitrogen.

X-ray diffraction data for DHFR crystals were collected at 100 K on a home source equipped with a RU300 rotating copper anode (Rigaku/MSC) and an R-axis IV++ detector. Data were processed using the d*trek program suite.[16] The reflection list was truncated and converted to CNS format using the CCP4 software suite.[17]

Structure refinement was performed using CNS software,[18] and manual model building was accomplished with the program O.[19] The initial model used in refinement was generated using the previously solved structure of DHFR with NADPH (PDB code 1RX1).[7] Because both crystals belonged to the same space group and shared similar unit cell parameters, it was not necessary to perform molecular replacement. Alternating rounds of manual rebuilding and model refinement were performed until *R* values and model geometry statistics were well within the acceptable range (see Table 1 and Results and Discussion). All figures illustrating structures were generated using the PyMOL Molecular Graphics System (DeLano Scientific).[20]

NMR Analysis of Compound 1. All spectra were recorded on a Bruker Avance 600 MHz NMR spectrometer. Proton spectra were acquired at 600.13 MHz using a 5 mm triple broadband inverse probe with *z*-axis gradient capability. The spectra were obtained in 16 scans in 64k data points over a 4.921 kHz spectral width. Sample temperature was maintained at 25 °C by a Bruker BVT 3000 digital variable temperature unit. A 1.5 s relaxation delay was used between acquisitions. The free induction decay (FID) was processed using exponential multiplication. The FID was also zero-filled to 128 K before Fourier transformation.

Carbon-13 NMR spectra were recorded at 150.92 MHz using the 5 ppm triple broadband inverse probe equipped with a *z*-axis gradient coil. The spectra were acquired over a 36.232 kHz spectral width in 32k data points. The ^{13}C pulse width was 4.6 μs (30° flip angle). A relaxation delay of 0.5 s was used. Edited ^{13}C spectra were obtained using the DEPT-135 pulse sequence with a composite 180° ^{13}C pulse during polarization transfer. The FIDs were processed using exponential multiplication and zero-filled to 128 K before Fourier transformation.

Compound **1** was dissolved in DMSO-d_6 (Cambridge Isotopes Laboratories Inc.) to a concentration of approximately 2.0 mg/mL. Chemical shifts were reported in ppm relative to TMS using the residual solvent signals at 2.50 and 39.52 ppm as internal references for the ^1H and ^{13}C spectra, respectively. Predicted ^{13}C chemical shift values were obtained using ACD Labs ^{13}C chemical shift prediction software (ver. 5.09).

Determination of the Inhibition Constant K_I of Compound 1 toward *E. coli* DHFR. To determine the inhibition constant (K_I)

for compound **1**, four concentrations of the inhibitor were tested: 2.5, 7.5, 25, and 75 nM. The second substrate NADPH was held at a saturating concentration (80 μM), while the variable substrate dihydrofolate was assayed at 10, 25, 50, 100, 150, 200, and 300 μM. Assays were performed at 25 °C in 50 mM Tris-HCl pH 7.5, containing 0.01% (w/v) Triton X-100 and 10 mM 2-mercaptoethanol. Reactions (200 μL) were initiated by the addition of purified *E. coli* DHFR to a final concentration of 5 nM. The oxidation of NADPH was monitored at 340 nm using a Molecular Devices SpectraMax Plus 96-well microtiter plate reading spectrophotometer. Plots were generated using SigmaPlot version 8.0 software and fit to the Michaelis−Menten equation for competitive inhibition (1):

$$v = V_{max}*[S]/K_M(1 + [I]/K_I) + [S] \quad (1)$$

Determination of IC_{50} Values. The DHFR inhibition observed with each derivative was characterized by determination and comparison of the IC_{50} values. IC_{50} determinations were performed as previously described[4] with 30 μM dihydrofolic acid, while tested compounds were varied from 0.0003 to 100 μM in triplicate. Data were curve-fit using GraFit version 4.0 (Erithacus software).

Compound Synthesis. All reagents were purchased from Aldrich Chemical Co. and used without further purification. Reactions were carried out under microwave irradiation using a Smith Synthesizer (Personal Chemistry). The equipment consisted of a continuous focused microwave power delivery system (0−300 W) that reaches and maintains a preselected temperature. Reactions were performed with stirring in 5 mL crimped, septum-sealed glass microwave vessels. Measured reaction times commenced when the solution reached the selected temperature (i.e., warming and cooling cycles were not included).

Mass spectra were obtained using a PE SCIEX API 2000 triple quadrupole MS with turboionspray ionization. All mass spectra were full-scan experiments (mass range 50−500 amu). The HPLC system was Shimadzu with an LC-8A pump and SPD-10A VP UV−vis system (λ = 230 nm) with ZorBAX (150 × 4.6 mm), and a mobile phase consisting of acetonitrile:water (70:30) with 0.1% TFA.

General Procedures for Amidinoisothiouronium Library Synthesis. Protocol A: Into a 5 mL microwave vessel were added 1 mL of CH_3CN followed by benzylchloride (0.5 mmol) and amidinothiourea (0.5 mmol, 1.0 equiv). After the vial was sealed, the mixture was stirred for 10 s and then irradiated between 85 and 100 °C for 5 min (see Table 3). After the mixture cooled to approximately 50 °C, the amidinoisothiouronium hydrochloride salt began to precipitate. The solid material was collected by filtration and washed twice with 1 mL of CH_3CN.

Protocol B: Into a 5 mL microwave vessel were added 1 mL of methanol followed by benzylchloride (0.5 mmol) and amidinothiourea (0.5 mmol, 1.0 equiv). After the vial was sealed, the mixture was stirred for 10 s and then irradiated at 60 °C for 20 min. After being cooled to room temperature, the solvent was removed in vacuo, and the residue was taken up in CH_3CN (1 mL) where the amidinoisothiouronium hydrochloride salt was allowed to slowly crystallize. The solid material was collected by filtration and washed twice with 1 mL of CH_3CN.

Protocol C: Into a 5 mL microwave vessel were added 1 mL of methanol followed by benzylchloride (0.5 mmol) and amidinothiourea (0.5 mmol, 1.0 equiv). After the vial was sealed, the mixture was stirred for 10 s and then irradiated at 60 °C for 20 min. After being cooled to room temperature, the solvent was removed in vacuo, and the residue was taken up in 1 mL of diethylether where crystallization was allowed to take place slowly. The desired amidinoisothiouronium hydrochloride salt was found to be contaminated by the amidinoisothiourea starting material. To remove the contaminant, the solid material was collected by filtration and washed twice with 1 mL of diethylether, then stirred in 1 mL of aqueous HCl 1 N at room temperature for 10 min, followed by collection via filtration and washing with H_2O (0.5 mL).

Protocol D: Into a 5 mL microwave vessel were added 1 mL of ethanol followed by bisbenzylchloride (0.5 mmol) and amidinothiourea (1.0 mmol, 2.0 equiv). After the vial was sealed, the mixture was stirred for 10 s and then irradiated at 90 °C for 5 min. After the mixture was cooled to approximately 50 °C, the bis(amidinoisothiouronium) dihydrochloride salt began to precipitate. The solid material was collected by filtration and washed twice with 1 mL of ethanol.

Acknowledgment. We thank Kalinka Koteva (Department of Biochemistry and Biomedical Sciences, McMaster University, Hamilton, ON) for mass spectrometric analysis of inhibitors. This work was supported by operating grants from The Canadian Bacterial Network and The Canadian Institutes of Health Research. E.B. holds a Canada Research Chair in Microbial Biochemistry. S.J. holds a Heart and Stroke Masters Studentship Award. We also thank the Ontario Research and Development Challenge Fund (ORDCF) for funding part of this work.

Supporting Information Available: General procedures for amidinoisothiouronium library synthesis; NMR and MS data and spectra for the library compounds. This material is available free of charge via the Internet at http://pubs.acs.org.

References

(1) Lee, H.; Reyes, V.; Kraut, J. Crystal Structures of *Escherichia coli* Dihydrofolate Reductase Complexed with 5-Formyltetrahydrofolate (Folinic Acid) in Two Space Groups: Evidence for Enolization of Pteridine O4. *Biochemistry* **1996**, *35*, 7012−7020.
(2) Koury, M. J.; Ponka, P. New Insights Into Erythropoieis: the Roles of Folate, Vitamin B12, and Iron. *Annu. Rev. Nutr.* **2004**, *24*, 105−131.
(3) Shane, B.; Stokstad, E. L. R. Vitamin B12−Folate Interrelationships. *Annu. Rev. Nutr.* **1985**, *5*, 115−141.
(4) Huennekens, F. M. The Methotrexate Story: a Paradigm for Development of Cancer Chemotherapeutic Agents. *Adv. Enzyme Regul.* **1994**, *34*, 397−419.
(5) Baccanaria, D. P.; Daluge, S.; King, R. W. Inhibition of Dihydrofolate Reductase: Effect of Reduced Nicotinamide Adenine Dinucleotide Phosphate on the Selectivity and Affinity of Diaminobenzylpyrimidines. *Biochemistry* **1982**, *21*, 5068−5075.
(6) Fierke, C. A.; Johnson, K. A.; Benkovic, S. J. Construction and Evaluation of the Kinetic Scheme Associated with Dihydrofolate Reductase From *Escherichia coli*. *Biochemistry* **1987**, *26*, 4085−4092.
(7) Sawaya, M. R.; Kraut, J. Strength of an Interloop Hydrogen Bond Determines the Kinetic Pathway in Catalysis by *Escherichia coli* Dihydrofolate Reductase. *Biochemistry* **1997**, *36*, 586−603.
(8) Zolli-Juran, M.; Cechetto, J. D.; Hartlen, R.; Daigle, D. M.; Brown, E. D. High Throughput Screening Identifies Novel Inhibitors of *Escherichia coli* Dihydrofolate Reductase that are Competitive with Dihydrofolate. *Bioorg. Med. Chem. Lett.* **2003**, *13*, 2493−2496.
(9) Then, R. L. Antimicrobial Dihydrofolate Reductase Inhibitors—Achievements and Future Options: Review. *J. Chemother.* **2004**, *16*, 3−12.
(10) Mayer, S.; Diagle, D. M.; Brown, E. D.; Khatri, J.; Organ, M. G. An Expedient and Facile One-Step Synthesis of a biguanide Library by Microwave Irradiation Coupled with Simple Product Filtration. Inhibitors of Dihydrofolate Reductase. *J. Comb. Chem.* **2004**, *6*, 776−782.
(11) Cummins, P. L.; Gready, J. E. Energetically Most Likely Substrate and Active-Site Protonation Sites and Pathways in the Catalytic Mechanism of Dihydrofolate Reductase. *J. Am. Chem. Soc.* **2001**, *123*, 3418−3428.
(12) Shrimpton, P.; Allemann, R. Role of Water in the Catalytic Cycle of *E. coli* Dihydrofolate Reductase. *Protein Sci.* **2002**, *11*, 1442−1451.
(13) Cannon, W.; Garrison, B.; Benkovic, S. Consideration of the pH-Dependent Inhibition of Dihydrofolate Reductase by Methotrexate. *J. Mol. Biol.* **1997**, *271*, 656−668.
(14) Gilbert, I. Inhibitors of Dihydrofolate Reductase in Leishmania and Trypanosomes. *Biochim. Biophys. Acta* **2002**, *587*, 249−257.
(15) Iwakura, M.; Furusawa, K.; Kokubu, T.; Ohashi, S.; Tanaka, Y.; Shimura, Y.; Tsuda, K. Dihydrofolate Reductase as a New "Affinity Handle". *J. Biochem.* **1992**, *111*, 37−45.
(16) Pflugrath, J. W. The Finer Things in X-ray Diffraction Data Collection. *Acta Crystallogr.* **1999**, *D55*, 1718−1725.

(17) Collaborative Computational Project Number 4. The CCP4 Suite: Programs for Protein Crystallography. *Acta Crystallogr*. **1994**, *D50*, 760−763.
(18) Brünger, A. T.; Adams, P. D.; Clore, G. M.; DeLano, W. L.; Gros, P.; Grosse-Kunstleve, R. W.; Jiang, J. S.; Kuszewski, J.; Nilges, M.; Pannu, N. S.; Read, R. J.; Rice, L. M.; Simonson, T.; Warren, G. L. Crystallography & NMR System: A New Software Suite for Macromolecular Structure Determination. *Acta Crystallogr*. **1998**, *D54*, 905−921.
(19) Jones, T. A.; Zou, J. Y.; Cowan, S. W.; Kjeldgaard, M. Improved Methods for Building Protein Models in Electron Density Maps and the Location of Errors in These Models. *Acta Crystallogr*. **1991**, *A47*, 110−119.
(20) DeLano, W. L. *The PyMol Molecular Graphics System*; DeLano Scientific: San Carlos, CA, 2002.

JM060570V